An experimental study of airfoil tip vortex formation noise

Danielle J. Moreau and Con J. Doolan

School of Mechanical & Manufacturing Engineering, UNSW, Sydney, Australia

ABSTRACT
This paper explores the noise produced by three-dimensional vortex flow at the tip of an airfoil. This noise source is an important component of the noise produced by aircraft high-lift systems. To investigate tip vortex formation noise, aeroacoustic measurements have been taken of a finite airfoil with flat ended tip in an anechoic wind tunnel at a range of flow speeds and angles of attack. Sound maps taken with a beamforming array are presented to show contributions of flow at the airfoil tip to overall airfoil noise production. Tip noise spectral data are also included to provide information about the nature of the noise source and scaling laws are developed of the noise generation process to model the noise data.

1. INTRODUCTION
The vortex generated at the tip of a finite airfoil such as an aircraft fixed wing, helicopter rotor or propeller blade can dominate its wake and be a significant source of flow-induced noise. Understanding the nature of this noise source is a necessary precursor to developing blade-tip designs that can reduce noise generation. While there have been many studies of tip vortex flow and in particular, the dynamics of the trailing tip vortex in far-field regions (Spalart, 1998; Lee and Pereira, 2010), few studies are concerned with the noise created by tip vortex formation which is the topic of this paper.

An airfoil tip vortex is characterized by the roll-up of vorticity shed from the trailing edge and the merging of co-rotating vortices that form on the tip surface. The tip vortex structure that forms at the flat ended tip of a NACA 0012 airfoil at an angle of attack is illustrated in Fig. 1. According to Bailey et al. (2006), the tip vortex consists of 3 distinct co-rotating vortices. Vortex A develops due to the flow of fluid from the pressure surface over the tip. Vortex B develops as the roll up of fluid along the suction side tip edge. Vortex C forms at the trailing edge tip due to slow-moving fluid on the pressure surface that rolls up towards the suction surface. At approximately half way along the chord, vortex A moves over to the suction surface tip edge and begins to interact with vortex B. Other studies have similarly identified the tip vortex structure to consist of multiple vortices that form on the tip surface, the number and arrangement of which depends on airfoil shape and tip geometry (Birch et al, 2004; Buffo et al, 2012; Giuni and Green, 2013). Downstream of the trailing edge, the multiple vortices all merge and interact, forming a trailing vortex that can persist in the far-field for thousands of chord lengths (Crow, 1970).

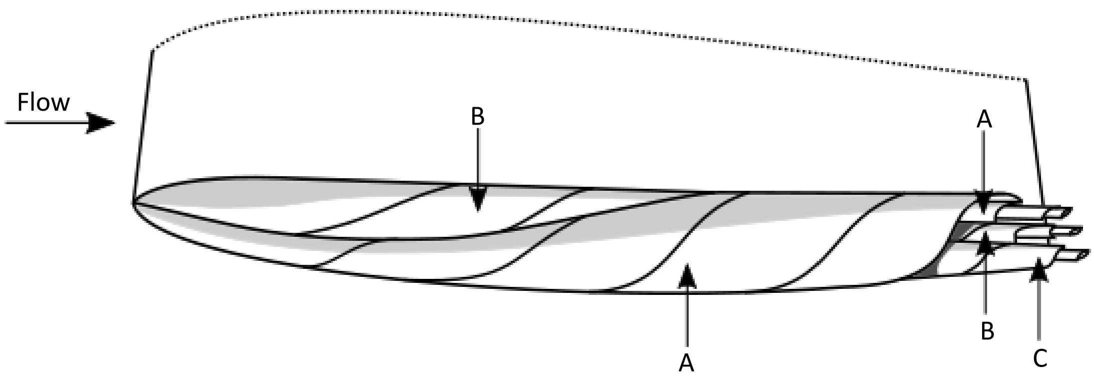

Figure 1: The tip vortex structure of a NACA 0012 with flat ended tip. Adapted from Bailey et al. (2006).

Available experimental data on airfoil tip vortex formation noise is scarce. Brooks and Marcolini (1986) are one of the few to measure tip noise from a finite airfoil. In their study, single point noise measurements were taken for a tripped NACA 0012 airfoil with rounded tip and aspect ratio (ratio of airfoil span, L, to chord, C) of L/C = 1 to 6 at Reynolds numbers of up to Re_C = 1 × 10^6, based on chord. Isolated tip noise measurements were obtained by comparing the sound generated by three-dimensional airfoils to that of their two-dimensional counterpart and a semi-empirical rounded tip noise model was developed. Using flat tip measurements (George and Chou, 1984), the semi-empirical tip noise model was later modified by Brooks et al. (1989) for applicability to an airfoil with a flat ended tip. Using the noise data of Brooks and Marcolini (1986), Mathias et al. (1998) examined the correlation of tip noise with mean tip flow parameters computed in RANS (Reynolds Averaged Navier Stokes) simulations at equivalent conditions to the experiments. The peak tip noise sound level was found to scale with the eighth power of velocity at the tip flow separation line. More recently, Klei et al. (2014) examined the noise produced at an airfoil tip with varying degrees of elliptical rounding. The wing model used in this study was an unswept Clark-Y profile with aspect ratio of L/C = 5. Microphone array measurements taken at Reynolds numbers of up to Re_C = 1.2 × 10^6 showed that low frequency noise levels were slightly reduced by tip rounding but the degree of elliptical rounding did not influence the level of noise reduction.

The aim of this paper is to present a high quality tip noise dataset obtained from an experimental campaign performed in the Stability Wind Tunnel at Virginia Tech. Acoustic measurements taken for a NACA 0012 airfoil with flat ended tip at Reynolds numbers of up to Re_C = 1.6 × 10^6 and for a range of angles of attack of α = 0 – 12° are presented to inform the acoustics community on the nature of the tip noise source (in terms of level and spectral content). The benchmark experimental data presented in this paper can be used in the future development and validation of tip noise predictions. It is worth noting that the results presented in this paper are the preliminary results of a much larger study examining this type of noise source.

2. METHODOLOGY

2.1 Experimental Facility

Experiments were performed in the anechoic test section of the Stability Wind Tunnel at Virginia Tech (in Virginia USA), shown in Fig. 2. This facility has low turbulence levels of up to 0.03% and can achieve flow speeds of up to 80 m/s depending on blockage. The test section has dimensions of 1.83 m × 1.83 m × 7.3 m and is shown in Fig. 3. The test section has tensioned Kevlar walls that contain the flow while being acoustically transparent. Sound generated in the test section passes through the Kevlar walls into two anechoic chambers located on either side of the test section where acoustic instrumentation can be placed.

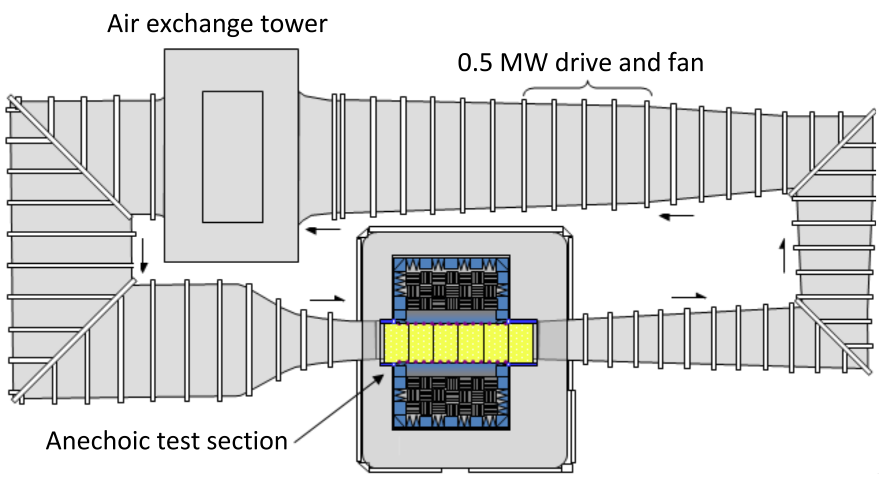

Figure 2: Stability Wind Tunnel with anechoic test section. Adapted from Alexander et al. (2013).

2.2 Test model

The test model consisted of a finite length NACA 0012 airfoil with flat ended tip and is shown in Fig. 4. The airfoil has a chord of C = 0.4 m, a span of L = 1.2 m and an aspect ratio of L/C = 3. As shown in Fig. 4, the airfoil was flush mounted to the wind tunnel ceiling so that the airfoil length axis (span) was perpendicular to the direction of the flow. Tests were performed with the airfoil tripped on both sides using serrated trip tape with 0.5 mm thickness at 10% chord.

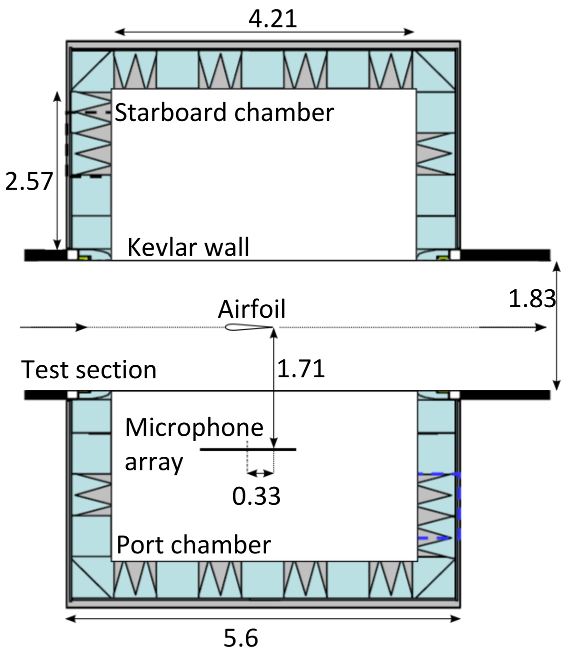

Figure 3: Experimental setup in the anechoic test section of the Stability Wind tunnel. Dimensions in m. Adapted from Devenport et al. (2013).

Figure 4: Airfoil model in the Stability Wind Tunnel test section.

2.3 Acoustic data acquisition and evaluation

An AVEC microphone array located in the port anechoic chamber was used to measure the sound emitted by the wall-mounted finite airfoil. The array has an outer diameter of 1.1 m and its centre was positioned 0.93 m above the test section floor. The location of the microphone array relative to the airfoil is shown in Fig. 3. The array consists of 117 Panasonic model WM-64PNT Electret microphones arranged in a 9-armed spiral. The 117 microphones were connected to an AVEC designed signal conditioning and filtering box and two 64-channel PCI-based data acquisition cards. Data from the 117 microphones were acquired at a sampling frequency of 51,200 Hz for a sample time of 32 s. Maps of local sound pressure contributions (or sound maps) were obtained using AVEC's post-processing algorithm and are displayed in 1/12th octave bands. In addition to sound maps, 1/12th octave band airfoil and tip noise spectra have been estimated by integrating the sound map over the entire airfoil and tip region. This integration process yields the sound pressure level as measured at the microphone array centre due to the sources contained in the integration regions. The sound map integration regions are shown in Fig. 5. In this figure, x is the streamwise direction where the flow is from left to right and y is the spanwise direction. A position of x = 0, y = 0 corresponds to the centre of the test section.

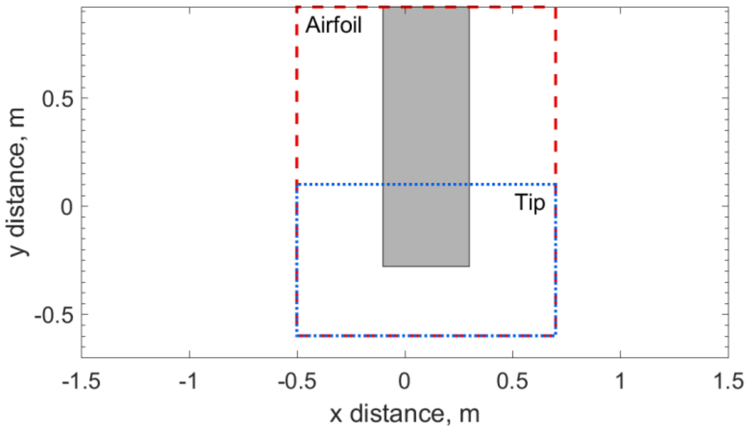

Figure 5: Airfoil and tip noise integration regions.

2.4 Test conditions

Experiments were conducted at free-stream velocities of U_∞ = 30 – 60 m/s corresponding to Reynolds numbers based on airfoil chord of Re_C = 7.9 × 10^5 – 1.6 × 10^6. Measurements were taken for an airfoil angle of attack of α = 0 – 12°.

To illustrate the tip vortex produced by the airfoil with flat ended tip in this study, Fig. 6 shows planes of mean velocity measured in the spanwise, wall-normal direction at U_∞ = 60 m/s. These measurements have been taken at 3.35 m or 8.4 chord lengths downstream of the airfoil trailing edge. In Fig. 6, z is the direction normal to the airfoil surface at α = 0°. A position of y = 0, z = 0 corresponds to the centre of the test section. A traversing wake rake containing 119 Pitot probes was used to measure the mean velocity planes in the airfoil wake. The rake consists of 112 Pitot probes and 7 Pitot static probes attached to a box shaped aluminum strut which encompasses the full cross-section of the test section (in the z direction). The 112 Pitot probes are made from 1.6 mm diameter stainless steel tubing while the Pitot static probes are Dwyer model 167 and have a diameter of 3 mm. The probes are connected to four DTC Initium ESP-32HD 32-channel pressure scanners with a range of ±2.5 psi.

In Fig. 6, the airfoil trailing edge can be identified as the thin central contour region with slight velocity deficit. The boundary layer that forms on the test section kevlar walls can also be observed at the extremities of the measurement plane. A tip vortex can be observed in Figs. 6(b) – (d) at non-zero angle of attack. The tip vortex size and radius of contour curvature increases with angle of attack. The mean velocity profiles display a minimum at the vortex core that is 77, 51 and 45% of the freestream velocity at α = 4, 8 and 12°, respectively. As the peak flow velocity in the vortex core is lower than freestream, the tip vortex is in a wakelike state at this measurement location.

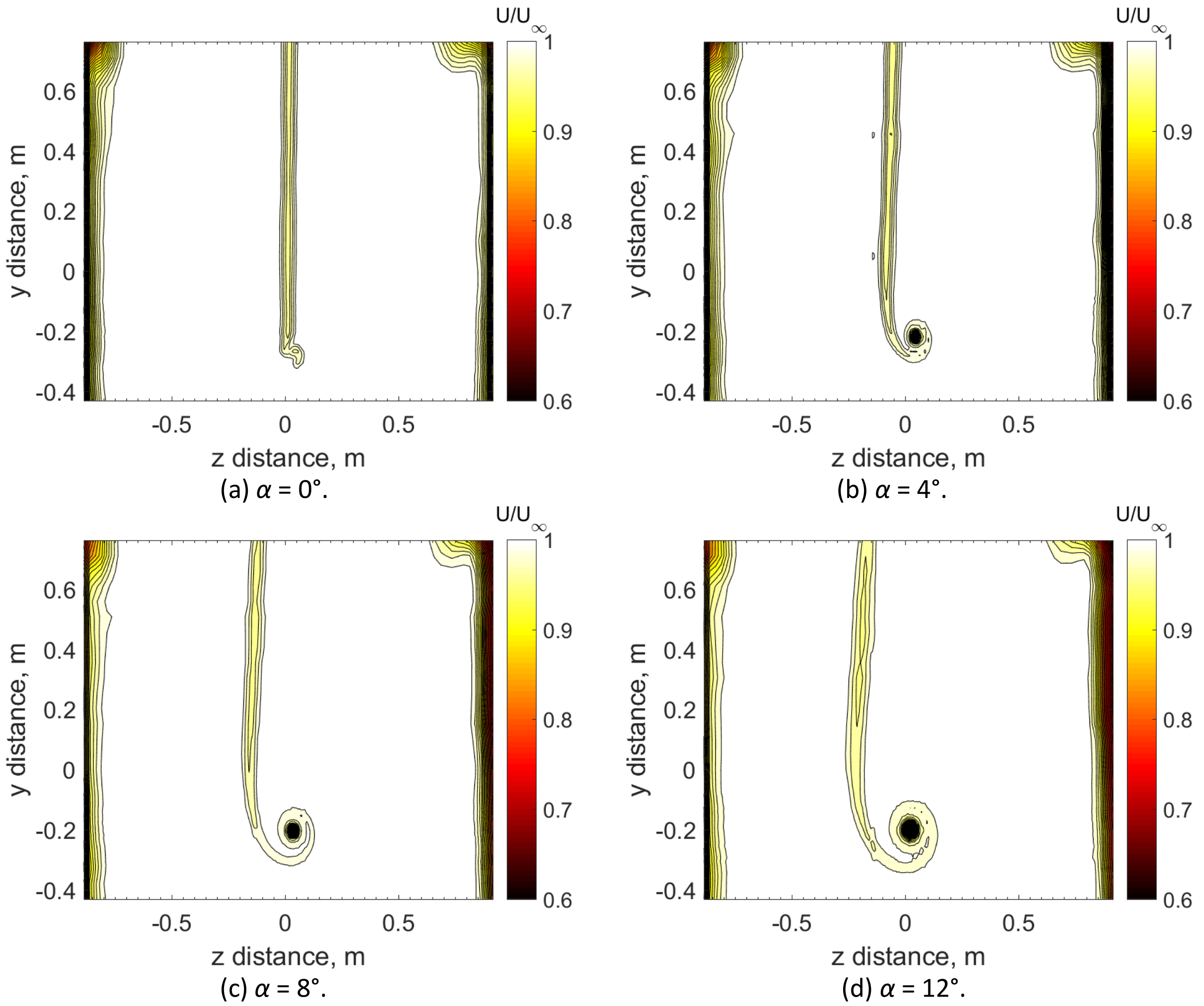

Figure 6: Normalised mean velocity contours in the airfoil wake at 8.4 chord lengths downstream of the airfoil trailing edge at U_∞ = 60 m/s.

3. RESULTS

Figures 7 – 9 present integrated airfoil and tip noise spectra along with beamforming sound maps. The sound maps in Fig. 9 are presented at the top flow speed of U_∞ = 60 m/s only. Sound maps are given in 1/12th octave band centre frequencies of 1.5 – 4.0 kHz and the location of the airfoil is shown in white.

The spectra in Figs. 7 and 8 show airfoil tip noise is measurable across the entire frequency range of interest. Comparing the total airfoil noise spectrum with that generated by the airfoil tip in Fig. 7 shows tip noise is a dominant source of high frequency airfoil noise. At the highest flow speed of U_∞ = 60 m/s, the sound maps in Fig. 9 show the airfoil tip is the dominant noise source location at frequencies of 2.8 kHz and above. Below this frequency, the airfoil trailing edge and leading edge-wall junction are dominant sources of airfoil noise. The sound maps also display significantly higher levels of tip noise at an angle of attack of α = 12° compared to the zero degree angle of attack case. Figures 7 and 8 show the dominant tip noise contribution manifests itself as a broad peak in the airfoil noise spectrum (i.e centred on 4.2 kHz at U_∞ = 60 m/s). The broad tip noise peak increases in amplitude as the angle of attack and to a lesser extent, flow speed, is increased. The frequency of the dominant tip noise contribution is also observed to reduce as flow speed is decreased (i.e. to 1.8 kHz at U_∞ = 30 m/s).

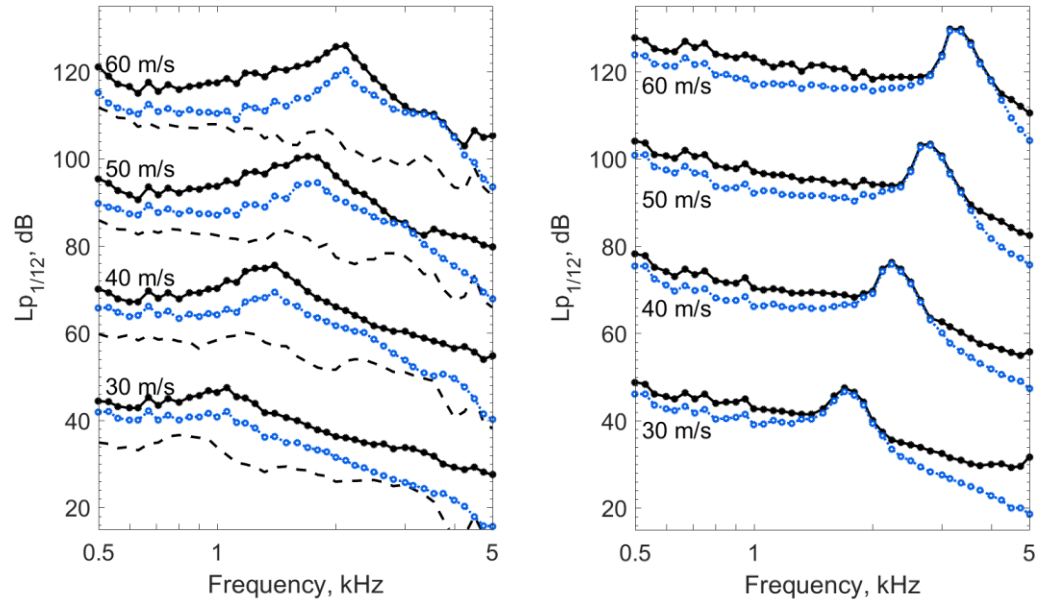

(a) α = 0°. (b) α = 12°.

Figure 7: Integrated 1/12th octave band airfoil and tip noise spectra at U_∞ = 30 – 60 m/s and α = 0 and 12°. The solid black line with filled circular markers is the airfoil spectrum while the dotted blue line with open circular markers is the tip noise spectrum. The dashed black line is the background noise spectrum of the empty tunnel. Note that with each increase in flow speed, the spectra have been offset by 20dB for clarity.

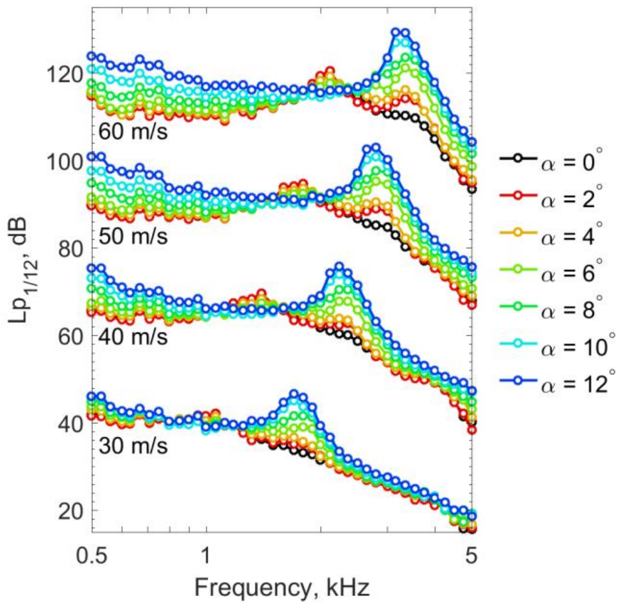

Figure 8: Integrated 1/12th octave band tip noise spectra for the airfoil at U_∞ = 30 – 60 m/s and α = 0 – 12°. Note that with each increase in flow speed, the spectra have been offset by 20dB for clarity.

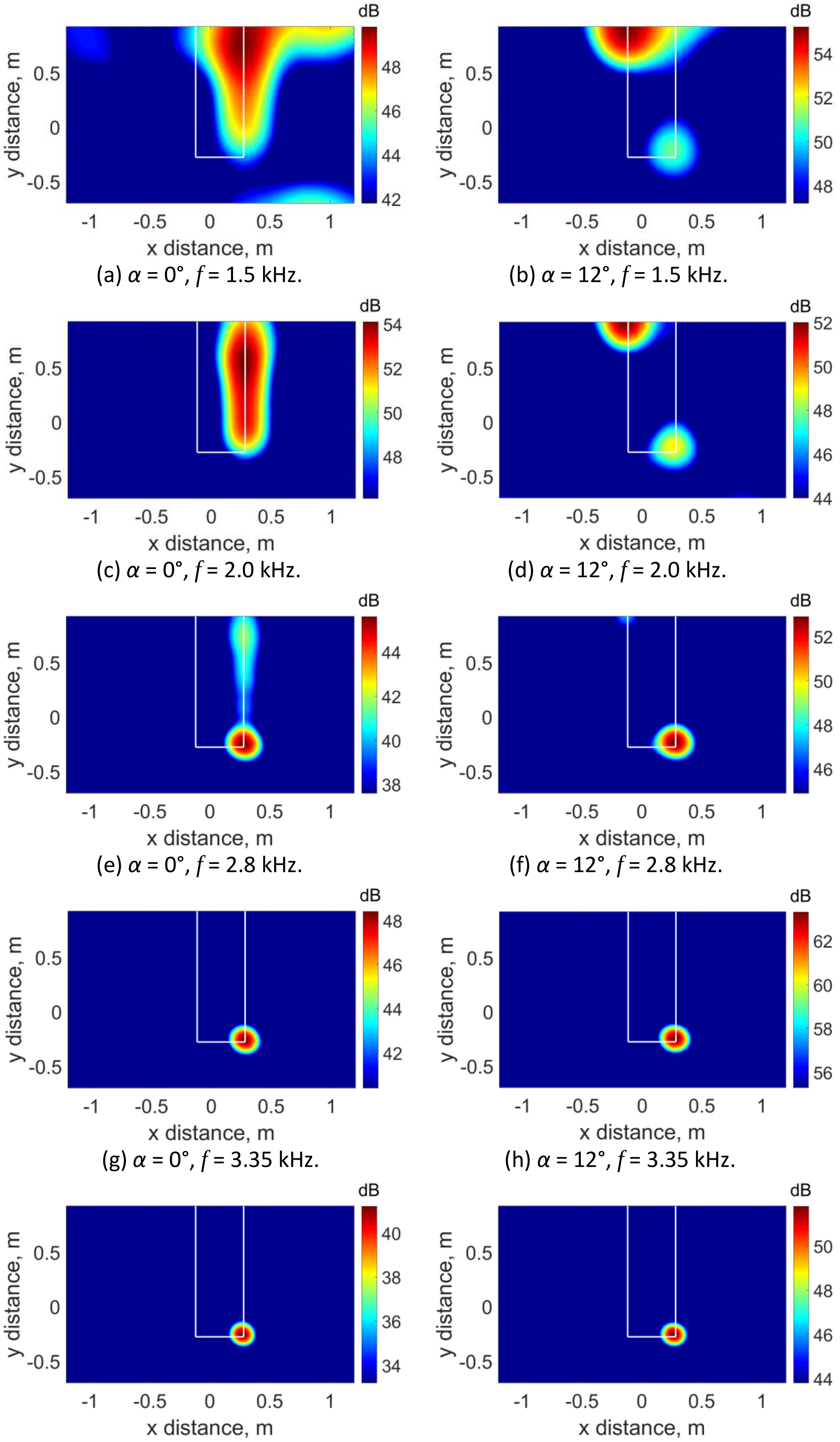

(a) α = 0°, f = 1.5 kHz. (b) α = 12°, f = 1.5 kHz.

(c) α = 0°, f = 2.0 kHz. (d) α = 12°, f = 2.0 kHz.

(e) α = 0°, f = 2.8 kHz. (f) α = 12°, f = 2.8 kHz.

(g) α = 0°, f = 3.35 kHz. (h) α = 12°, f = 3.35 kHz.

(h) α = 0°, f = 4.0 kHz. (i) α = 12°, f = 4.0 kHz.

Figure 9: Sound maps for the airfoil at U_∞ = 60 m/s and α = 0 and 12°.

Velocity scaling can be used to understand the nature of the underlying tip noise source. A common scaling employed in airfoil noise studies is M^5 where M is the free-stream Mach number. According to Ffowcs Williams and Hall, the amplitude of noise radiated by a (non-compact) semi-infinite flat plate with sharp trailing edge scales proportionally with M^5. Figure 10 shows 1/12th octave band tip noise spectra normalised by

$$Lp_{1/12\ \mathrm{Scaled1}} = Lp_{1/12} - 10\log_{10}(M^5) \tag{1}$$

where $Lp_{1/12}$ is the tip noise spectrum. The frequency of noise is expected to scale according to $f \sim U_\infty/l$, where l is the characteristic length scale. In Fig. 10, airfoil chord, C, is used as the characteristic length scale and the normalised spectra are plotted against Strouhal number based on chord, $St_C = fC/U_\infty$.

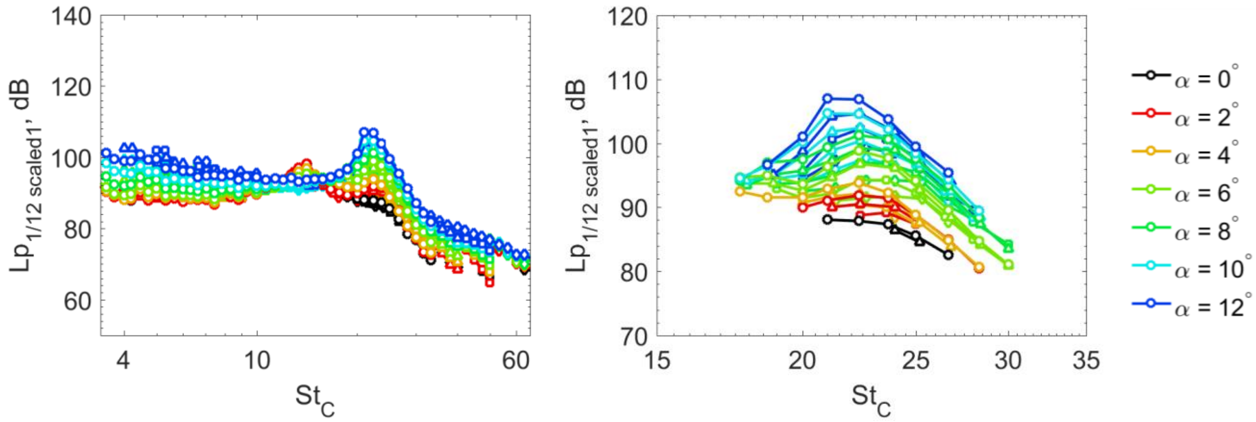

(a) Tip noise spectra. (b) Dominant tip noise contribution.

Figure 10: Normalised tip noise spectra at U_∞ = 30 – 60 m/s and α = 0 – 12° scaled with Eqn. (1). Markers '◊', '□', 'Δ' and 'o', denote flow speeds of U_∞ = 30, 40, 50 and 60 m/s, respectively.

In Fig. 10(a), the tip noise spectra of Fig. 8 are normalized according to Eqn. (1) while Fig. 10(b) shows normalisation of the dominant component of the tip noise spectrum only. That is, only portions of the tip noise spectrum that are within 1 dB of the total airfoil noise spectrum (see Fig. 7) are normalised in Fig. 10(b).

Figure 10 shows the frequency of the dominant tip noise peak scales with Strouhal number and is centred on $St_C = 23$. In Fig. 10(a), the broadband component of the tip noise spectrum at $St_C < 10$ and $St_C > 30$ collapses with M^5 scaling at each angle of attack. This suggests that low and high frequency components of tip noise are due to trailing edge scattering of vorticity in the tip region. The dominant tip noise peak in Fig. 10(b) does not show a good collapse with M^5 scaling. This indicates that at frequencies where tip noise is the dominant airfoil noise mechanism, the tip noise source cannot simply be attributed to an enhancement of trailing edge noise due to increased turbulence and the formation of vortices at the tip.

Figure 11 shows tip noise spectra normalised by

$$Lp_{1/12\ \mathrm{Scaled2}} = Lp_{1/12} - 10\log_{10}(M^{7.5}) \tag{2}$$

where a Mach number power dependency of 7.5 has been calculated to give the least mean squared error between scaled dominant tip noise contributions at each angle of attack. While this scaling law does not collapse the tip noise spectra over the entire frequency range of interest (see Fig. 11(a)), the dominant tip noise peak scales well with $M^{7.5}$ at each angle of attack (see Fig. 11(b)). The tip noise peak therefore displays a Mach number dependence of $M^{7.5}$ which is higher than the well-known edge-scattering scaling of M^5 for trailing edge noise. Mathias et al. (1998) also found a similar Mach number dependence of M^8 when scaling the tip noise data of Brooks and Marcolini (1986).

Figure 11(b) displays an offset between velocity scaled dominant tip noise contributions measured at different angles of attack. This may be due some directionality of the noise source which means that noise is rotated with the model at an angle of attack. Alternatively, an additional term accounting for the angle of attack dependence may be

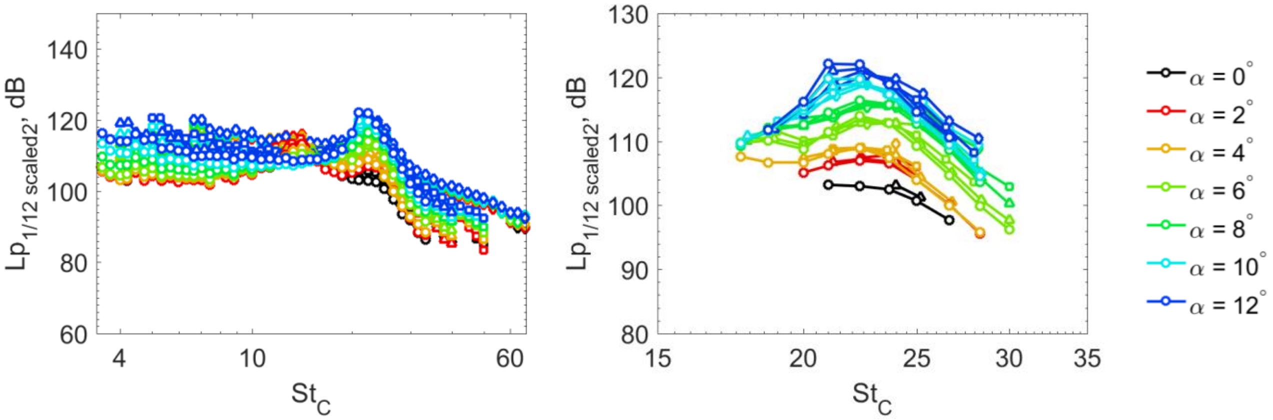

(a) Tip noise spectra. (b) Dominant tip noise contribution.

Figure 11: Normalised tip noise spectra at U_∞ = 30 – 60 m/s and α = 0 – 12° scaled with Eqn. (2). Markers '◊', '□', 'Δ' and 'o', denote flow speeds of U_∞ = 30, 40, 50 and 60 m/s, respectively.

needed to completely normalise the dominant tip noise contribution. Figure 12 shows excellent collapse of the dominant tip noise peak is obtained at all angles of attack and flow speeds when employing the following scaling law

$$Lp_{1/12\ \mathrm{Scaled3}} = \begin{cases} Lp_{1/12} - 10\log_{10}(M^{7.5}), & \alpha = 0 \\ Lp_{1/12} - 10\log_{10}(M^{7.5}) - 10\log_{10}\left(\alpha_{Tip}^{2.5}\right), & \alpha > 0 \end{cases} \quad (3)$$

This scaling law has been derived to give the least mean squared error between scaled dominant tip noise contributions by incorporating a power law dependency on the effective angle of attack at the tip, α_{Tip}. This parameter was calculated by determining the spanwise effective angle of attack distribution for the airfoil using the general formulation of Prandtl's classical lifting-line theory for a rectangular planform wing (Katz and Plotkin, 2001). The tip noise scaling law of Eqn. (3) is at this stage only preliminary and further study is needed to confirm its general applicability.

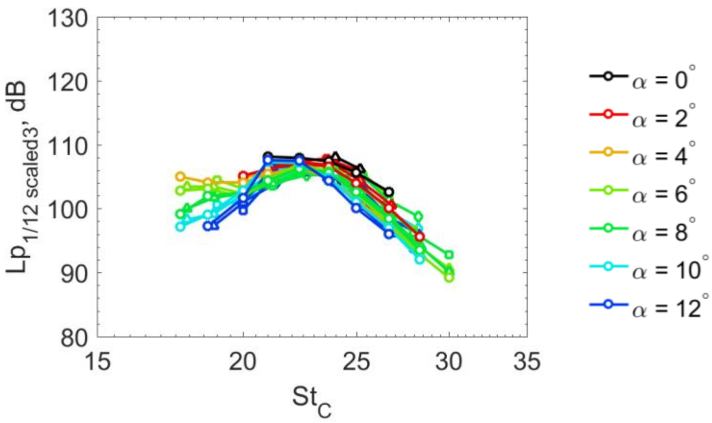

Figure 12: Dominant tip noise contribution at U_∞ = 30 – 60 m/s and α = 0 – 12° scaled with Eqn. (3). Markers '◊', '□', 'Δ' and 'o', denote flow speeds of U_∞ = 30, 40, 50 and 60 m/s, respectively.

4. CONCLUSION

This paper has examined the noise produced by the flat ended tip of a NACA 0012 airfoil. The results include sound maps taken with a microphone array and spectral data for the individual noise contribution from the airfoil tip to overall airfoil noise generation. The results, while preliminary, shed light upon the nature of tip noise production. The broadband component of the tip noise spectrum at St_C < 10 and St_C > 30 collapses with a Mach number power dependence of 5 at each angle of attack indicating that tip noise in the low and high frequency range is due to trailing edge scattering of vorticity in the tip region. A broad peak is also present in the tip noise spectrum centred on St_C = 23 that displays a Mach number power dependence of 7.5 and an angle of attack power dependence of 2.5. This investigation is part of an ongoing study to obtain a comprehensive database of experimental tip flow field and noise data for a variety of different tip shapes to improve understanding of the tip noise generation mechanism.

ACKNOWLEDGEMENTS

This work has been supported by the Australian Research Council under LP110100033 and DE150101528, the Australian-American Fulbright Commission, the Sir Ross and Sir Keith Smith Fund and the South Australian Premier's Research and Industry Fund Catalyst Research Grant Program. In addition, the authors would like to thank Dr Nathan Alexander, Timothy W. Meyers, Prof. William J. Devenport, Bill Oejtens, Dr Aurelien Borgoltz and Dr Nanya Intaratep for their valuable assistance during the experimental test campaign.

REFERENCES

Alexander, WN, Devenport, W, Morton, MA & Glegg, SAL 2013, 'Noise from a rotor ingesting a planar turbulent boundary layer', 19th AIAA/CEAS Aeroacoustics Conference, AIAA 2013 – 2285, Berlin, Germany.

Bailey, SCC, Tavoularis, S & Lee, BHK 2006, 'Effects of freestream turbulence on wing-tip vortex formation and near field', *Journal of Aircraft*, vol. 43, no. 5, pp. 1282 – 1291.

Birch, D, Lee, T, Mokhtarian, F and Kafyeke, F 2004, 'Structure and induced drag of a tip vortex', *Journal of Aircraft*, vol. 41, no. 5, pp. 1138 – 1145.

Brooks, TF & Marcolini, MA 1986, 'Airfoil Tip Vortex Formation Noise', *AIAA Journal*, vol. 24, no. 2, pp. 246 – 252.

Brooks, TF, Pope, D & Marcolini, M 1989, 'Airfoil Self Noise and Prediction', NASA TR – 1218.

Buffo, RM, Wolf, CC, Dufhaus, S, Hoernschemeyer, R & Stumpf, E 2012, 'Vortex creation and wing-tip geometry dependencies', 30th AIAA Applied Aerodynamics Conference, AIAA 2012 – 2770, New Orleans, LA.

Crow SC 1970, 'Stability theory for a pair of trailing vortices', *AIAA Journal*, vol. 8, no. 12, pp. 2172 – 2179.

Devenport, WJ, Burdisso, RA, Borgoltz, A, Ravetta, PA, Barone, MF, Brown, KA & Morton, MA 2013, 'The Kevlar-walled anechoic wind tunnel', *Journal of Sound and Vibration*, vol. 332, pp. 3971 – 3991.

Ffowcs Williams JE & Hall LH 1970, 'Aerodynamic sound generation by turbulent flow in the vicinity of a scattering half plane', *Journal of Fluid Mechanics*, vol. 40, pp. 657 – 670.

Giuni, M & Green, RB 2013, `Vortex formation on squared and rounded tip', *Aerospace Science and Technology*, vol. 29, pp. 191 – 199.

George, AR, and Chou, S-T 1984, 'Broadband Rotor Noise Analyses', NASA TR CR – 3797.

Katz J & Plotkin A, 2001, *Low-speed Aerodynamics*, 2nd Ed, Cambridge University Press, Cambridge UK.

Klei, CE, Buffo, RM & Stumpf, E 2014, 'Effects of wing tip shaping on noise generation', Inter-noise 2014, Melbourne, Australia.

Lee, T & Pereira, J 2010, 'Nature of wakelike and jetlike axial tip vortex flows', *Journal of Aircraft*, vol. 47, no. 6, pp. 1946 – 1954.

Mathias, DL, Pye, JD & Catwell, BJ 1998, 'Correlation of wingtip noise with mean flow parameters', 16th AIAA Applied Aerodynamics Conference, AIAA 98 – 2738, Albuquerque, NM.

Spalart, PR 1998, 'Airplane trailing vortices', *Annual Review of Fluid Mechanics*, vol. 30, pp. 135 – 143.